Transmissive Ultrathin Pancharatnam-Berry Metasurfaces with nearly 100% Efficiency

Weijie Luo,[1] Shulin Sun,[2,†] He-Xiu Xu,[1] Qiong He,[1,3] and Lei Zhou[1,3,*]

[1]*State Key Laboratory of Surface Physics and Key Laboratory of Micro and Nano Photonic Structures (Ministry of Education), Fudan University, Shanghai 200433, China*

[2]*Shanghai Engineering Research Center of Ultra-Precision Optical Manufacturing, Green Photonics and Department of Optical Science and Engineering, Fudan University, Shanghai 200433, China*

[3]*Collaborative Innovation Center of Advanced Microstructures, Nanjing 210093, China*

(Received 28 September 2016; revised manuscript received 1 March 2017; published 28 April 2017)

Pancharatnam-Berry (PB) metasurfaces exhibit strong abilities to control spin-polarized light, but *transmission*-mode PB functional devices exhibiting simultaneously *nearly 100%* efficiencies and *ultrathin* thicknesses are rarely seen. Here, we show that 100%-efficiency photonic spin Hall effect (PSHE) can be realized in *ultrathin* PB metasurfaces exhibiting both electric and magnetic responses satisfying certain criteria, and then we design and fabricate a microwave transmissive PB metasurface with thickness of approximately $\lambda/8$ yet exhibiting a maximum PSHE efficiency of approximately 91% in experiments (approximately 94% in full-wave simulations). Our results can stimulate the realizations of high-performance PB metadevices with diversified functionalities at different frequencies. As an example, we fabricate several vortex-beam generators and demonstrate that they not only exhibit ultrahigh working efficiencies but also are immune from normal-mode background interferences.

DOI: 10.1103/PhysRevApplied.7.044033

I. INTRODUCTION

The photonic spin Hall effect (PSHE), that a spin-polarized light can change its propagation direction depending on the "spin" that it carries, has attracted extensive attention recently [1–11]. Other than the *intrinsic* PSHE caused by the spin-orbit couplings [1–4], the PSHE can also be induced by the *extrinsic spin-dependent* light scatterings at Pancharatnam-Berry (PB) metasurfaces—ultrathin metamaterials (MTMs) constructed by planar electromagnetic (EM) resonators with orientations rotated successively [5–11] [see Fig. 1(b)]. However, the efficiencies of extrinsic PSHE generated by *transmission-mode ultrathin* PB metasurfaces were typically very low: only a small portion of input light can be deflected anomalously after passing through the devices. Such low-efficiency issue persists in PB devices exhibiting other functionalities (e.g., vortex-beam generators [12,13] and metaholograms [11,14,15]).

In a recent paper, we show that the efficiency of extrinsic PSHE can approach 100% if the Jones matrix of the unit element satisfies certain criteria [8], which is verified by experiments in *reflection* geometry in different frequency domains [8,16–18]. However, for *transmission* geometry, which is more useful in practice, experimental realizations of nearly 100%-efficiency PSHE were difficult, especially in *ultrathin* metasurfaces with thickness nearly an order of magnitude smaller than the wavelength [19–21]. Although the efficiencies of PB *dielectric* metasurfaces can be remarkably high, their thicknesses are comparable to the wavelength [22–27]. As a result, *ultrathin* PB metadevices with very high efficiencies (nearly 100%) and diversified functionalities are rarely seen.

In this work, we first employ Jones-matrix and effective-current analyses to understand that adding effective magnetic responses to the meta-atom design is crucial to realize the nearly 100%-efficiency PSHE with an ultrathin PB device, which is in the same spirit as previous high-transmission arguments in different scenarios [28–51]. Based on these understandings, we design and fabricate a microwave PB metasurface with thickness of approximately $\lambda/8$ and experimentally demonstrate that its PSHE efficiency reaches 91%. Our findings can help understand previous diversified results on PSHE in PB *transmissive* metasurfaces, which can inspire other spin-related photonic applications. As an example, we experimentally demonstrate that PB metadevices designed based on our criteria can be *highly efficient* in generating optical vortexes without suffering interferences with normal-field background.

II. RESULTS AND DISCUSSION

A. Criteria to achieve 100%-efficiency PSHE based on a generalized surface-current analysis

We start by analyzing the PSHE efficiency of a generic PB metasurface as shown in Fig. 1. For simplification, we assume that the basic meta-atom exhibits mirror

*Corresponding author.
phzhou@fudan.edu.cn
†Corresponding author.
sls@fudan.edu.cn

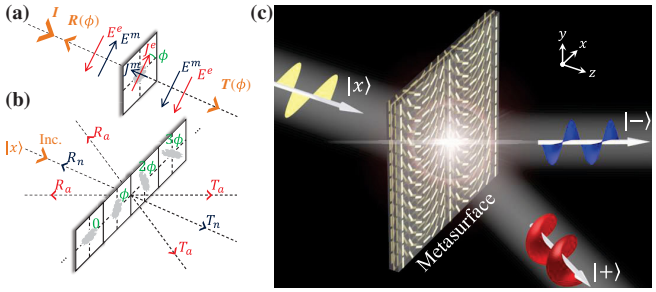

FIG. 1. (a) Schematics of a ϕ-oriented meta-atom with transmission and reflection characteristics described by two Jones matrices $\mathbf{T}$ and $\mathbf{R}$, and the E fields radiated from the electric and magnetic currents ($\vec{J}^e$ and $\vec{J}^m$) generated on the meta-atom. (b) Anomalous and normal transmissions and reflections (with efficiencies of T_a, R_a, T_n, R_n) generated by a generic PB metasurface consisting of meta-atoms with spatially varying orientation angles $(0, \phi, 2\phi, 3\phi\ldots)$ under illumination of a linearly polarized incident beam. (c) Schematics of the 100%-efficiency PSHE achieved by a PB metasurface satisfying Eq. (2), with $|x\rangle$, $|+\rangle$, $|-\rangle$ representing beams with linear polarization, left circular polarization, and right circular polarization, respectively.

symmetries so that its EM properties can be described by two Jones matrices $T = \mathrm{diag}(t_{uu}, t_{vv})$ and $R = \mathrm{diag}(r_{uu}, r_{vv})$ with u and v denoting its two principle axes. As the PB metasurface is shined by a spin-polarized beam, its scatterings generate four beams, which are normal or anomalous transmission or reflection modes, respectively. Figure 1(b) schematically depicts the light scatterings on a PB metasurface illuminated by a *linearly* polarized (LP) light. According to the theory presented in Ref. [8], the efficiencies of these four beams are

$$T_n \equiv |(t_{uu} + t_{vv})|^2/4, \qquad R_n \equiv |(r_{uu} + r_{vv})|^2/4,$$
$$T_a \equiv |(t_{uu} - t_{vv})|^2/4, \qquad R_a \equiv |(r_{uu} - r_{vv})|^2/4, \tag{1}$$

where the subscripts "n" and "a" stand for the normal and anomalous modes, respectively. Therefore, a 100%-efficiency transmissive PSHE can be realized if the constitutional meta-atom satisfies the following condition (see the Supplemental Material [52]):

$$r_{uu} = r_{vv} = 0, \quad |t_{uu}| = |t_{vv}| = 1, \quad \arg(t_{uu}) = \arg(t_{vv}) \pm \pi. \tag{2}$$

We now argue that condition (2) can be reached in a system with both (*effective*) electric and magnetic responses but *not* in a system with only *electric* responses. We follow Ref. [20] to model a layer of our meta-atoms as a *homogeneous* metasurface carrying *effective* electric surface currents $J^e_\alpha = A^{-1}\int (j_\alpha + \partial D_\alpha/\partial t)d\tau$ and magnetic ones $J^m_\alpha = A^{-1}\int (\partial B_\alpha/\partial t)d\tau$, where $\alpha = u, v$ and the integrations are performed within a unit cell with A being its surface area. These surface currents are proportional to the *local* $\mathbf{E}$ and $\mathbf{B}$ fields, which are, in turn, proportional to the incident EM field. We, thus, define two susceptibility matrices such that $J^e_\alpha = (Z_0^{-1})\chi^e_\alpha E^i_\alpha$, $J^m_\alpha = Z_0\chi^m_\alpha H^i_\alpha$ where Z_0 is the vacuum impedance, and "i" stands for the incident field. With these definitions, we analytically derive the transmission and reflection coefficients of the model, utilizing the following boundary conditions: $\vec{n}\times(\vec{H}_1 - \vec{H}_2) = \vec{J}^e$, $\vec{n}\times(\vec{E}_1 - \vec{E}_2) = -\vec{J}^m$ for EM fields across the metasurface. Assuming that the metasurface is freely standing in air, we get [52]

$$t_{uu} = 1 - \frac{1}{2}\chi^e_u - \frac{1}{2}\chi^m_v, \qquad t_{vv} = 1 - \frac{1}{2}\chi^e_v - \frac{1}{2}\chi^m_u,$$
$$r_{uu} = -\frac{1}{2}\chi^e_u + \frac{1}{2}\chi^m_v, \qquad r_{vv} = -\frac{1}{2}\chi^e_v + \frac{1}{2}\chi^m_u. \tag{3}$$

Equation (3) can be understood in a physical way. The E fields radiated from an electric or magnetic surface current are symmetrical or antisymmetrical at two sides of the current source [see Fig. 1(a)]. Therefore, in a system having both *electric* and *magnetic* responses, waves radiated from two surface currents can *constructively* interfere at the transmission side but *destructively* interfere at the reflection side, which is the case in Eq. (3). Therefore, the presence of both electric and magnetic responses provides more freedom to tune the transmission or reflection characteristics of the meta-atom *independently*, in sharp contrast to the model studied in Refs. [19,21] where only the *electric* response is considered (i.e., $\chi^m_i \equiv 0$) [52]. We note that the above arguments are in the same spirit as previous discussions on high-transmission structures although performed in different scenarios [28–51].

Such expanded tuning freedom helps us realize the 100%-efficiency PSHE. If we put Eq. (2) into Eq. (1), we can rigorously prove that when the susceptibilities of our meta-atoms satisfy [52]

$$\chi^e_u = \chi^m_v = 1 + e^{i\delta}, \qquad \chi^e_v = \chi^m_u = 1 + e^{i(\delta\pm\pi)}, \tag{4}$$

with δ being an arbitrary angle, we have $T_n = R_n = R_a = 0$ and $T_a = 1$, which is the 100%-efficiency PSHE as desired [see Fig. 1(c)]. The crucial role played by the magnetic current is, thus, clear. First, it helps match the impedances of our meta-atom with air, making it *reflectionless* for arbitrary polarizations [42,43]. Second, further tuning its electric and magnetic responses can make our meta-atom behave as a half-wavelength wave plate, as required by Eq. (2).

B. Design, fabrication, and characterizations of the meta-atom

Having understood the role of *magnetic* current, we now design our PB meta-atom to achieve 100%-efficiency PSHE in transmission geometry. A naive approach is to add

free-standing split-ring resonators into our design, but that makes the designed meta-atom very complicated, and it becomes *nonflat* on the x-y plane [43]. Here, we focus on designing *flat* meta-atoms with magnetic responses introduced in an *effective* way. We note that high *magnetic* fields can be stimulated in the gap between two electric MTM layers under certain conditions [44]. We also note that multilayered structures have been used to design transmissive meta-atoms [28–51], but our design presented below exhibits better performance and thinner thickness. We follow Ref. [46] to study the ABA structure with A and B being two electric MTM layers [see Fig. 2(a) inset]. Figure 2(a) depicts how the transmission amplitude $|t|$ of the ABA structure varies against the permittivities of two

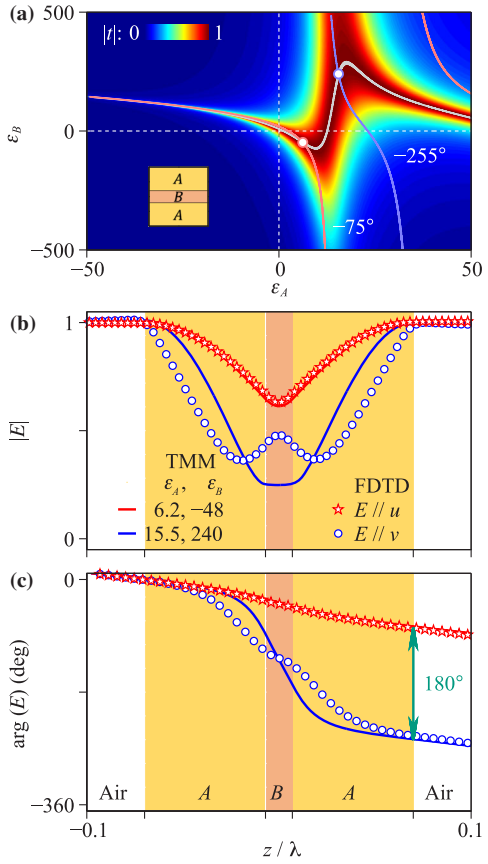

FIG. 2. (a) Transmission amplitude and two equal-transmission-phase lines in the $\varepsilon_A - \varepsilon_B$ diagram for the ABA model (see inset) with the thicknesses of two layers as $d_A/\lambda = 0.063$ and $d_B/\lambda = 0.014$ calculated by the transfer-matrix method (TMM) at wavelength λ. Evolutions of the (b) amplitude and (c) phase of the electric field inside the model ABA structure (with $\varepsilon_A^u = 6.2$, $\varepsilon_B^u = -48$, $\varepsilon_A^v = 15.5$, $\varepsilon_B^v = 240$) and the realistic ABA structure (see the Fig. 3 caption details) illuminated by normally incident EM waves polarized along two principle axes at 10.5 GHz calculated by the TMM (for the model) and FDTD simulations (for the realistic structure). Field integrations over the x-y plane within a unit cell are performed to obtain the FDTD results. We set $d_A = 1.8$ mm and $d_B = 0.4$ mm in the model ABA structure.

layers ε_A and ε_B with the thicknesses d_A and d_B of two layers fixed. Clearly, perfect transmission ($|t| = 1$) can happen in different phase regions when the condition

$$Z_A^2\left[2 - \tan(k_A d_A)\tan(k_B d_B)\frac{Z_A}{Z_B} + \frac{\tan(k_B d_B)}{\tan(k_A d_A)}\frac{Z_B}{Z_A}\right] = 2 - \tan(k_A d_A)\tan(k_B d_B)\frac{Z_B}{Z_A} + \frac{\tan(k_B d_B)}{\tan(k_A d_A)}\frac{Z_A}{Z_B} \quad (5)$$

is satisfied [44,46]. Here, $Z_i = 1/\sqrt{\varepsilon_i}$ and $k_i = \sqrt{\varepsilon_i}\omega/c$ with $i = A, B$. Moreover, the $|t| = 1$ line can intersect with different equal-phase lines at different positions [46]. Therefore, we choose two equal-phase lines with a π phase difference to intersect with the $|t| = 1$ line and find that Eq. (2) can be satisfied if we choose our meta-atom with $\varepsilon_A^u = 6.2$, $\varepsilon_B^u = -48$ and $\varepsilon_A^v = 15.5$, $\varepsilon_B^v = 240$. These values indicate that our meta-atom is a highly *anisotropic* trilayer structure with appropriately chosen effective-medium parameters. Figures 2(b) and 2(c) further illustrate how the amplitude and phase of electric fields evolve inside such an ABA structure, which is shined by normally incident EM waves with two polarizations. Indeed, EM waves with both polarizations can perfectly transmit through the meta-atom, but the accumulated phases of the transmitted waves exhibit a difference of π. The inherent physics is that perfect transparencies for two polarizations are governed by two different mechanisms so that the associated transmission phases are naturally different [45]. While the transparency for the $\vec{E}\|\hat{u}$ case is governed by the scattering cancellation mechanism [44], the mechanism for another polarization turns to be the Fabry-Perot resonance [46].

These effective-medium parameters help us design a realistic meta-atom in the microwave regime. Layer A can be realized by an anistropic resonator since its effective ε_A^u and ε_A^v are both positive, and, thus, we adopt a metallic bar in our design [see Fig. 3(a)]. Layer B is more difficult to design since its ε_B^u and ε_B^v exhibit different signs. We choose a composite structure consisting of a holey metallic film (which provides a negative-ε background) coupled with a metallic bar (which provides a positively large ε for one polarization) to design the B structure [see Fig. 3(a)]. Two dielectric spacers are used to separate these metallic layers when forming the ABA structure, and all structural details are carefully optimized based on finite-difference time-domain (FDTD) simulations [52]. Note the thickness of the ABA meta-atom is only 4 mm (approximately $\lambda/8$). We fabricate the single-A and-B layers and the final ABA structure based on the design, and Fig. 3(b) shows the pictures of the fabricated A and B layers. We measure the transmission characteristics of the ABA structure and individual A and B layers. As shown in Figs. 3(c) and 3(e), within a frequency window (10.1–10.9 GHz), the ABA structure is optically transparent for both polarizations

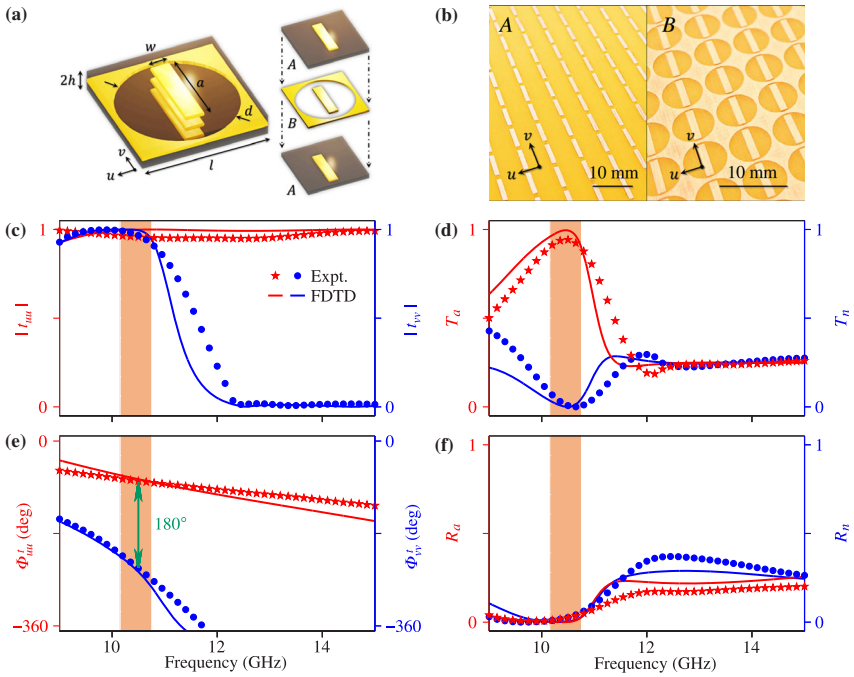

FIG. 3. (a) Schematics of the *ABA* meta-atom and individual *A* structure and *B* structure. Dielectric spacers with thickness $h = 2$ mm and $\varepsilon = 4.6$ are adopted to separate three metallic structures to form the final *ABA* meta-atom. (b) Pictures of the fabricated layer *A* (left) and layer *B* (right). Measured and FDTD simulated spectra of transmission (c) amplitude and (e) phase for a metasurface consisting of a periodic array of *ABA* meta-atoms (with periodicity 7×7 mm^2). Efficiencies of (d) anomalous or normal transmissions and (f) anomalous or normal reflections for a PB metasurface constructed with the *ABA* meta-atoms studied in (c),(e) calculated with Eq. (1) based on measured or simulated, transmission or reflection characteristics of the meta-atom. Here, $a = 5.8$ mm, $w = 1.1$ mm, $d = 6.5$ mm.

with the transmission-phase difference of approximately 180°. FDTD simulations are in good agreement with the experimental results of both the *ABA* structure [solid lines in Figs. 3(c) and 3(e)] and the individual *A* and *B* layers [52]. In particular, their effective-medium parameters match well with the required theoretical values [52] evidenced also by the good agreement between the field patterns calculated with the FDTD simulations and the effective-medium analysis [Fig. 2(b)]. We put the Jones-matrix parameters [Figs. 3(c) and 3(e)] into Eq. (1) to get the predicted efficiencies of the four beams (T_a, T_n, R_a, R_n) for a PB metasurface made by such a meta-atom. Figures 3(d) and 3(f) show that the predicted efficiency of the anomalous transmission T_a can approach 100% within 10.1–10.9 GHz, with all other energy channels suppressed nearly completely ($T_n \approx R_a \approx R_n \approx 0$).

More physics can be gained by checking the (*effective*) magnetic currents generated inside the structure. We calculate the effective susceptibilities of the meta-atom according their mathematical definitions based on integrating the EM fields obtained in the FDTD simulations. As shown in Fig. 4, our specifically designed meta-atom can excite appropriate magnetic currents inside the structure with amplitudes matching those of the electric currents and phases satisfying the 100%-efficiency criterion Eq. (4), within the frequency interval of 10.1–10.9 GHz [52].

C. Photonic spin Hall effect and vortex-beam generators

We now use the meta-atom designed in Sec. II B to construct two different types of PB metasurfaces and experimentally characterize their excellent spin-dependent wave-manipulation performance (e.g., PSHE and vortex-beam generations). We first study the PSHE effect and verify the theoretical predictions presented in Fig. 3. Using the *ABA* structure as the basic element, we fabricate a PB metasurface with interparticle rotation angle $\phi = 30°$ [see Fig. 5(a)] and then experimentally characterize its PSHE properties. In our experiments, we shine a LP microwave normally onto the metasurface and then measure its scattering patterns using two horn antennas, which can receive, respectively, EM waves with left circular polarization (LCP) (denoted as $|+\rangle$) and right circular polarization (RCP) ($|-\rangle$). Figures 5(b)–5(f) depict the measured

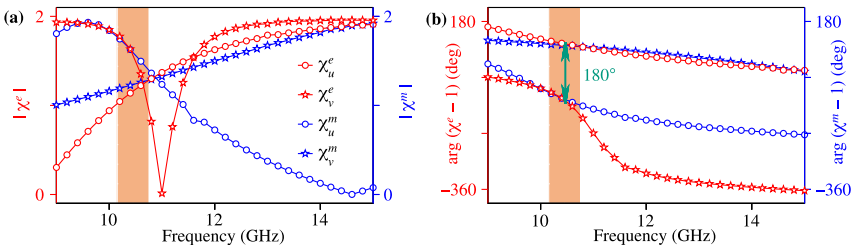

FIG. 4. Spectra of (a) amplitudes and (b) phases of the electric and magnetic susceptibilities of our meta-atom obtained by integrating FDTD-simulated electric or magnetic current distributions inside the structure illuminated by normally incident plane waves with polarizations along the $\hat{u}$ and $\hat{v}$ axes.

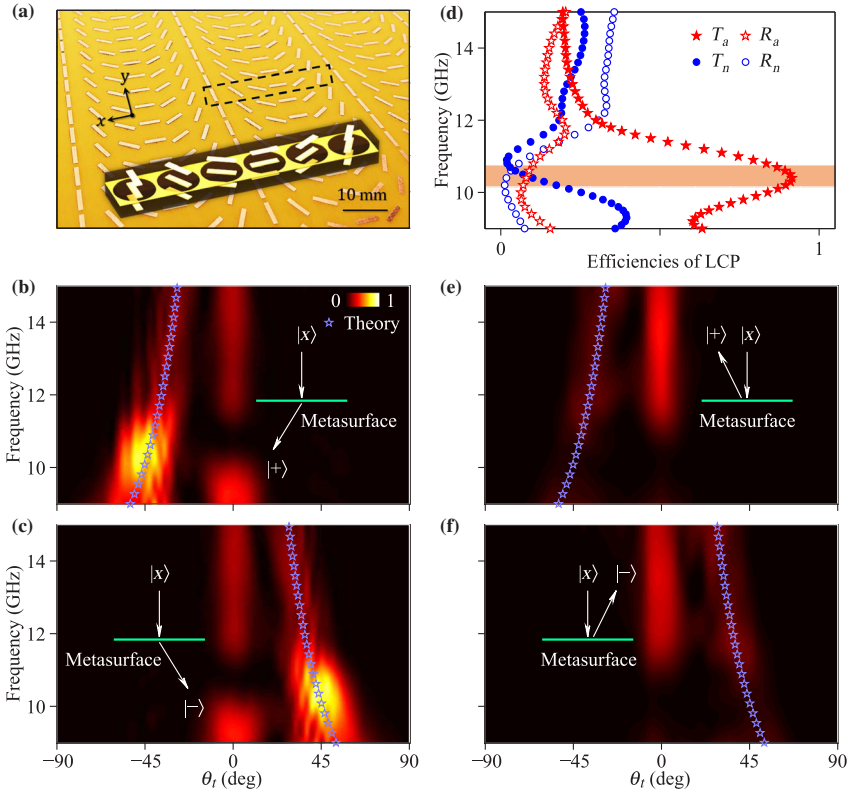

FIG. 5. (a) Picture of fabricated PB metasurface formed by the *ABA* meta-atoms studied in Fig. 3. Measured scattered-field intensities (color map) in the (b),(c) transmission and (e),(f) reflection sides versus the frequency and the detecting angle for the PB metasurface illuminated by normally incident LP beams. The receivers are circularly polarized antennas with polarization (b),(f) LCP and (c),(e) RCP, respectively. (d) Absolute efficiencies of the four modes versus frequency for the PB metasurface obtained by integrations over the appropriate angle regions of different modes based on the experimental data in (b),(c),(e),(f). Blue stars in (b),(c),(e),(f) represent the results obtained based on the generalized Snell's law.

spin-sensitive scattering patterns of our sample at both transmission and reflection sides. All data are normalized against the signals transmitted through an aperture with the same size as that of the metasurface measured by a LCP antenna. Figures 5(b)–5(f) show that within 10.1–10.9 GHz, only the anomalous transmissions survive with all other three modes significantly suppressed. Outside this band, the anomalous-transmission efficiency gradually decreases. Figure 5(d) depicts the efficiencies of all four modes versus frequency, which are obtained from the experimental data through integrations over the angle regions of the considered modes [8]. Consistent with the Jones-matrix analysis [Figs. 3(d) and 3(f)], the measured PSHE efficiency of our PB metasurface reaches a maximum (approximately 91%) at 10.5 GHz. We also perform FDTD simulations of realistic systems to study their PSHE properties. As shown in Fig. 6, the FDTD results reproduce the experimental results well, showing that the maximum PSHE efficiency can reach 94%. The slight difference between the measured and simulated values can be attributed to the sample imperfections and the nonideal performance of our antennas. We emphasize that the condition [i.e., Eq. (4)] to achieve 100%-efficiency PSHE is derived for uniform metasurfaces (without microstructures) under normal-incidence excitations. In practice, where the designed PB metasurfaces (such as that in Fig. 5) are always composed by nonuniform microstructures, such 100%-efficiency claim is approximately valid only when the direction of the transmitted wave does not significantly deviate from that of the incident wave, as in our case (the deflection angle 45° is not large). In general, the meta-atoms must exhibit more complex properties (such as bianisotropic response [31] or asymmetric structure [32]) in order to achieve high-efficiency large-angle anomalous refractions.

Our designed meta-atom can be used to realize other high-performance *transmission-mode* PB devices. As an example, we construct three vortex-beam generators and experimentally characterize their performance. As shown in Figs. 7(a), 7(d), and 7(g), our vortex-beam generators are constructed by a collection of meta-atoms with that at the point (x, y) exhibiting an orientation angle ϕ satisfying $\phi = (q/2)\tan(y/x)$. Here, q is an integer denoting the topological charge [12,53–56]. In our experiments, we shine these devices by normally incident RCP beams emitted from a horn placed 1.0 m away, and we use a 1.5-cm-long monopole antenna to measure the $\mathrm{Re}(E_x)$ distributions on an x-y plane 50 cm below the metasurfaces at the transmission side. Figures 7(b), 7(e), and 7(h) show that the three devices can generate *pure* vortex beams with $q = 1, 2, 3$ at 10.5 GHz, formed by interferences among anomalous-mode waves passing through meta-atoms at different positions [54,55]. However, if we repeat the measurements at 14.5 GHz, the obtained beams are no longer *pure* vortex beams with patterns obviously blurred and field strengths significantly weakened [see Figs. 7(c), 7(f), and 7(i)]. The physics can be easily understood from the intrinsic properties of the designed meta-atom as shown

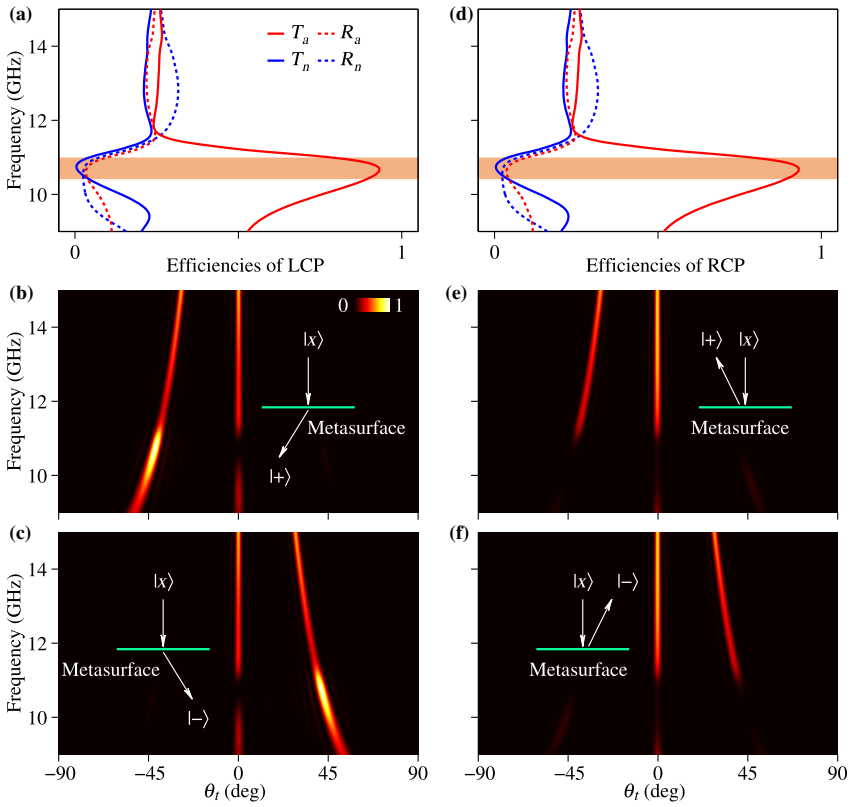

FIG. 6. FDTD-simulated scattered-field intensities (color map) in the (b),(c) transmission and (e),(f) reflection regions versus the frequency and detecting angle for the PB metasurface illuminated by the normally incident LP beams. Simulated absolute efficiencies of the four modes in the cases where the metasurfaces are illuminated by (a) RCP and (d) LCP beams. The maximum value of T_a is 94% at 10.5 GHz.

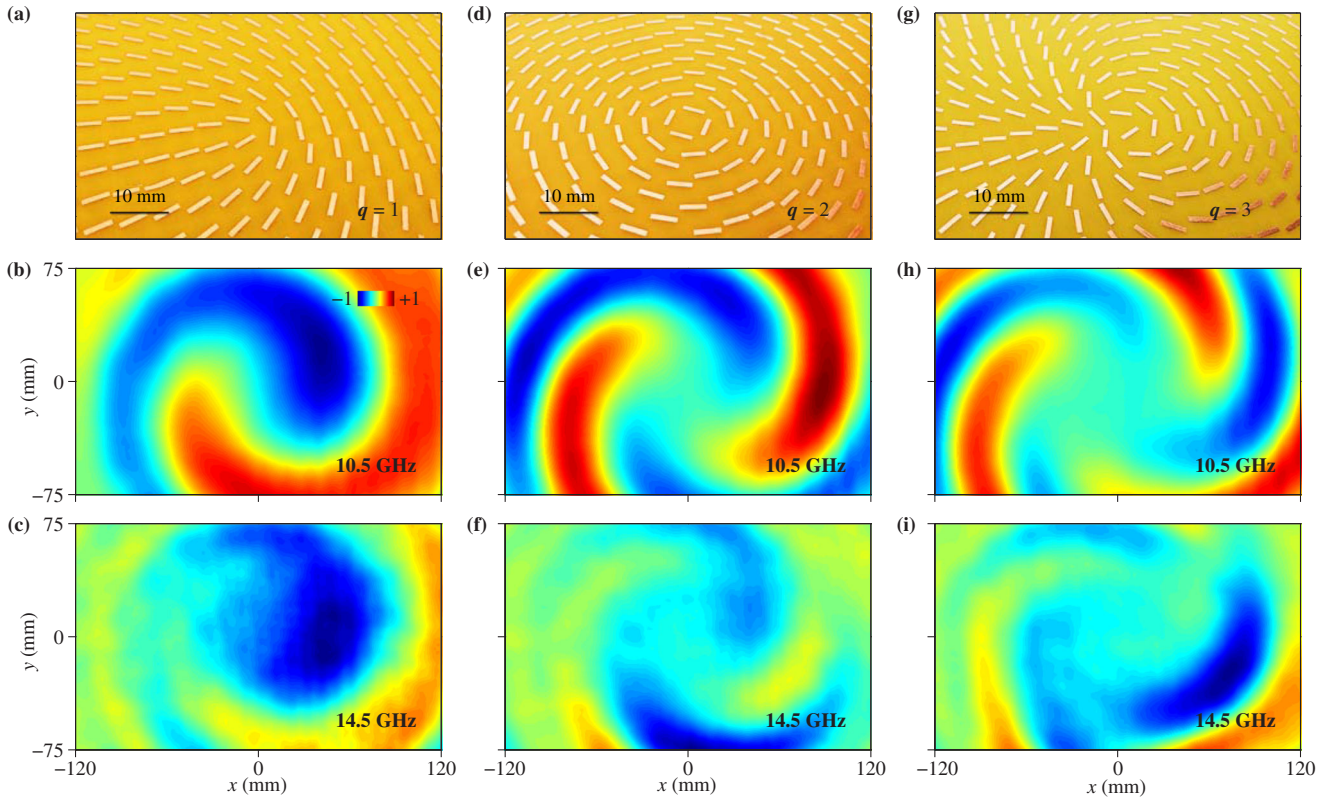

FIG. 7. Pictures of fabricated vortex-beam generators with topological charge (a) $q = 1$, (d) $q = 2$, and (g) $q = 3$ constructed with the *ABA* meta-atom studied in Fig. 3. Measured $\mathrm{Re}(E_x)$ distributions on an x-y plane 50 cm below two metasurfaces, which are shined by normally incident RCP waves at (b),(e),(h) 10.5 GHz and (c),(f),(i) 14.5 GHz.

in Figs. 3(d) and 3(f). Out of the working band (10.1–10.9 GHz), our meta-atom supports not only *anomalous* transmissions (with efficiency T_a) with PB phases but also *normal* transmission (with efficiency T_n) without PB phases, not mentioning the reflections [see Figs. 3(d) and 3(f)]. Therefore, at frequencies out of the working band, the normal-mode background not only lowers the vortex-generation efficiency but also interferes with the vortex beams generated by the anomalous modes, which explains the deteriorated performance shown in Figs. 7(c), 7(f), and 7(i).

III. CONCLUSION

In summary, within an extended model framework in which both electric and magnetic responses are considered, we show that nearly 100%-efficiency PSHE can be realized in lossless transmissive PB metasurfaces with electric and magnetic responses satisfying certain criteria. These criteria guide us to design a microwave metasurface based on a trilayer structure (with total thickness much less than the wavelength) and experimentally demonstrate that the maximum achievable PSHE efficiency can reach 91%. Our results can stimulate realizing other PB metadevices with high efficiencies and performance, with three vortex-beam generators experimentally demonstrated here as an illustration. Extensions to high-frequency domains are exciting, and a possible design is presented in the Supplemental Material [52].

ACKNOWLEDGMENTS

This work is supported by the National Natural Science Foundation of China (Grants No. 11474057, No. 11404063, No. 11674068, and No. 61501499) and the Shanghai Science and Technology Committee (Grants No. 16ZR1445200 and No. 16JC1403100).

[1] M. Onoda, S. Murakami, and N. Nagaosa, Hall Effect of Light, Phys. Rev. Lett. **93**, 083901 (2004).
[2] K. Y. Bliokh and Y. P. Bliokh, Conservation of Angular Momentum, Transverse Shift, and Spin Hall Effect in Reflection and Refraction of an Electromagnetic Wave Packet, Phys. Rev. Lett. **96**, 073903 (2006).
[3] O. Hosten and P. Kwiat, Observation of the spin Hall effect of light via weak measurements, Science **319**, 787 (2008).
[4] X. Yin, Z. Ye, J. Rho, Y. Wang, and X. Zhang, Photonic spin Hall effect at metasurfaces, optical spin Hall effects in plasmonic chains, Science **339**, 1405 (2013).
[5] N. Shitrit, I. Bretner, Y. Gorodetski, V. Kleiner, and E. Hasman, Optical spin Hall effects in plasmonic chains, Nano Lett. **11**, 2038 (2011).
[6] L. Huang, X. Chen, B. Bai, Q. Tan, G. Jin, T. Zentgraf, and S. Zhang, Helicity dependent directional surface plasmon polariton excitation using a metasurface with interfacial phase discontinuity, Light Sci. Appl. **2**, e70 (2013).
[7] J. Lin, J. P. B. Mueller, Q. Wang, G. Yuan, N. Antoniou, X. Yuan, and F. Capasso, Polarization-controlled tunable directional coupling of surface plasmon polaritons, Science **340**, 331 (2013).
[8] W. Luo, S. Xiao, Q. He, S. Sun, and L. Zhou, Photonic spin Hall effect with nearly 100% efficiency, Adv. Opt. Mater. **3**, 1102 (2015).
[9] M. Khorasaninejad and K. B. Crozier, Silicon nanofin grating as a miniature chirality-distinguishing beam-splitter, Nat. Commun. **5**, 5386 (2014).
[10] Y. Li, J. Zhang, S. Qu, J. Wang, H. Chen, L. Zheng, Z. Xu, and A. Zhang, Achieving wideband polarization-independent anomalous reflection for linearly polarized waves with dispersionless phase gradient metasurfaces, J. Phys. D **47**, 425103 (2014).
[11] S. Xiao, F. Zhong, H. Liu, S. Zhu, and J. Li, Flexible coherent control of plasmonic spin-Hall effect, Nat. Commun. **6**, 8360 (2015).
[12] L. Huang, X. Chen, H. Mu, G. Li, and B. Bai, Dispersionless phase discontinuities for controlling light oropagation, Nano Lett. **12**, 5750 (2012).
[13] Y. Yang, W. Wang, P. Moitra, I. I. Kravchenko, D. P. Briggs, and J. Valentine, Dielectric meta-reflectarray for broadband linear polarization conversion and optical vortex generation, Nano Lett. **14**, 1394 (2014).
[14] L. Huang, X. Chen, H. Mühlenbernd, H. Zhang, S. Chen, B. Bai, Q. Tan, G. Jin, K.-W. Cheah, C.-W. Qiu, J. Li, T. Zentgraf, and S. Zhang, Three-dimensional optical holography using a plasmonic metasurface, Nat. Commun. **4**, 2808 (2013).
[15] P. Genevet and F. Capasso, Holographic optical metasurfaces: A review of current progress, Rep. Prog. Phys. **78**, 024401 (2015).
[16] G. Zheng, H. Mühlenbernd, M. Kenney, G. Li, T. Zentgraf, and S. Zhang, Metasurface holograms reaching 80% efficiency, Nat. Nanotechnol. **10**, 308 (2015).
[17] S. Jiang, X. Xiong, Y. Hu, S. Jiang, Y. Hu, D. Xu, R. Peng, and M. Wang, High-efficiency generation of circularly polarized light via symmetry-induced anomalous reflection, Phys. Rev. B **91**, 125421 (2015).
[18] M. Tymchenko, J. S. Gomez-diaz, J. Lee, N. Nookala, M. A. Belkin, and A. Alù, Gradient Nonlinear Pancharatnam-Berry Metasurfaces, Phys. Rev. Lett. **115**, 207403 (2015).
[19] A. Alu, Wave-shaping surfaces, Physics **6**, 53 (2013).
[20] A. Arbabi and A. Faraon, Fundamental limits of ultrathin metasurfaces, arXiv:1411.2537.
[21] X. Ding, F. Monticone, K. Zhang, L. Zhang, D. Gao, S. N. Burokur, A. de Lustrac, Q. Wu, C.-W. Qiu, and A. Alù, Ultrathin Pancharatnam-Berry metasurface with maximal cross-polarization efficiency, Adv. Mater. **27**, 1195 (2015).
[22] D. Lin, P. Fan, E. Hasman, and M. L. Brongersma, Dielectric gradient metasurface optical elements, Science **345**, 298 (2014).
[23] R. C. Devlin, M. Khorasaninejad, W. T. Chen, J. Oh, and F. Capasso, Broadband high-efficiency dielectric metasurfaces for the visible spectrum, Proc. Natl. Acad. Sci. U.S.A. **113**, 10473 (2016).

[24] M. Khorasaninejad, W. T. Chen, R. C. Devlin, J. Oh, A. Y. Zhu, and F. Capasso, Metalenses at visible wavelengths: Diffraction-limited focusing and subwavelength resolution imaging, Science **352**, 1190 (2016).
[25] Q.-T. Li, F. Dong, B. Wang, F. Gan, J. Chen, Z. Song, L. Xu, W. Chu, Y.-F. Xiao, Q. Gong, and Y. Li, Polarization-independent and high-efficiency dielectric metasurfaces for visible light, Opt. Express **24**, 16309 (2016).
[26] S. Kruk, B. Hopkins, I. Kravchenko, A. Miroshnichenko, D. N. Neshev, and Y. S. Kivshar, Broadband highly-efficient dielectric metadevices for polarization control, APL Photonics **1**, 030801 (2016).
[27] L. Wang, S. Kruk, H. Tang, T. Li, I. Kravchenko, D. N. Neshev, and Y. S. Kivshar, Grayscale transparent metasurface holograms, Optica **3**, 1504 (2016).
[28] C. Pfeiffer and A. Grbic, Millimeter-wave transmitarrays for wavefront and polarization control, IEEE Trans. Microwave Theory Tech. **61**, 4407 (2013).
[29] M. Selvanayagam and G. V. Eleftheriades, Discontinuous electromagnetic fields using orthogonal electric and magnetic currents for wavefront manipulation, Opt. Express **21**, 14409 (2013).
[30] A. Epstein and G. V. Eleftheriades, Floquet-Bloch analysis of refracting Huygens metasurfaces, Phys. Rev. B **90**, 235127 (2014).
[31] V. S. Asadchy, M. Albooyeh, S. N. Tcvetkova, A. Diaz-Rubio, Y. Radi, and S. A. Tretyakov, Perfect control of reflection and refraction using spatially dispersive metasurfaces, Phys. Rev. B **94**, 075142 (2016).
[32] J. P. S. Wong, A. Epstein, and G. V. Eleftheriades, Reflectionless wide-angle refracting metasurfaces, IEEE Antennas Wireless Propag. Lett. **15**, 1293 (2016).
[33] V. S. Asadchy, I. A. Faniayeu, Y. Ra'di, S. A. Khakhomov, I. V. Semchenko, and S. A. Tretyakov, Broadband Reflectionless Metasheets: Frequency-Selective Transmission and Perfect Absorption, Phys. Rev. X **5**, 031005 (2015).
[34] N. M. Estakhri and A. Alù, Recent progress in gradient metasurfaces, J. Opt. Soc. Am. B **33**, A21 (2016).
[35] S. B. Glybovski, S. A. Tretyakov, P. A. Belov, Y. S. Kivshar, and C. R. Simovski, Metasurfaces: From microwaves to visible, Phys. Rep. **634**, 1 (2016).
[36] K. Achouri, B. A. Khan, S. Gupta, G. Lavigne, M. A. Salem, and C. Caloz, Synthesis of electromagnetic metasurfaces: Principles and illustrations, Eur. Phys. J. Appl. Metamater. **2**, 12 (2015).
[37] S. A. Tretyakov, Metasurfaces for general transformations of electromagnetic field, Phil. Trans. R. Soc. A **373**, 20140362 (2015).
[38] A. Epstein and G. V. Eleftheriades, Huygens' metasurfaces via the equivalence principle: Design and applications, J. Opt. Soc. Am. B **33**, A31 (2016).
[39] A. Epstein and G. V. Eleftheriades, Arbitrary power-conserving field transformations with passive lossless omega-type bianisotropic metasurfaces, IEEE Trans. Antennas Propag. **64**, 3880 (2016).
[40] Y. He and G. V. Eleftheriades, Rotated infrared antenna transmitarray for the manipulation of circularly polarized wavefronts, Eur. Phys. J. Appl. Metamater. **1**, 8 (2014).
[41] S. L. Jia, X. Wan, D. Bao, Y. J. Zhao, and T. J. Cui, Independent controls of orthogonally polarized transmitted waves using a Huygens metasurface, Laser Photonics Rev. **9**, 545 (2015).
[42] F. Monticone, N. M. Estakhri, and A. Alù, Full Control of Nanoscale Optical Transmission with a Composite Metascreen, Phys. Rev. Lett. **110**, 203903 (2013).
[43] C. Pfeiffer and A. Grbic, Metamaterial Huygens' Surfaces: Tailoring Wave Fronts with Reflectionless Sheets, Phys. Rev. Lett. **110**, 197401 (2013).
[44] L. Zhou, W. Wen, C. Chan, and P. Sheng, Electromagnetic-Wave Tunneling Through Negative-Permittivity Media with High Magnetic Fields, Phys. Rev. Lett. **94**, 243905 (2005).
[45] W. Sun, Q. He, J. Hao, and L. Zhou, A transparent metamaterial to manipulate electromagnetic wave polarizations, Opt. Lett. **36**, 927 (2011).
[46] W. Sun, Q. He, S. Sun, and L. Zhou, High-efficiency surface plasmon meta-couplers: Concept and microwave-regime realizations, Light Sci. Appl. **5**, e16003 (2016).
[47] R. H. Phillion, S. Member, and M. Okoniewski, Lenses for circular polarization using planar arrays of rotated passive elements, IEEE Trans. Antennas Propag. **59**, 1217 (2011).
[48] D. Zelenchuk and V. Fusco, Split-ring FSS spiral phase plate, IEEE Antennas Wireless Propag. Lett. **12**, 284 (2013).
[49] C. Pfeiffer and A. Grbic, Controlling Vector Bessel Beams with Metasurfaces, Phys. Rev. Applied **2**, 044012 (2014).
[50] C. Liu, Y. Bai, Q. Zhao, Y. Yang, H. Chen, J. Zhou, and L. Qiao, Fully controllable Pancharatnam-Berry metasurface array with high conversion efficiency and broad bandwidth, Sci. Rep. **6**, 34819 (2016).
[51] A. Niv, G. Biener, V. Kleiner, and E. Hasman, Manipulation of the Pancharatnam phase in vectorial vortices, Opt. Express **14**, 4208 (2006).
[52] See Supplemental Material http://link.aps.org/supplemental/10.1103/PhysRevApplied.7.044033 for the derivations of Eqs. (2)–(4), 25% efficiency limit for metasurfaces with purely electric responses, effective-medium analyses of the proposed meta-atom, additional experimental and simulation results of the meta-atom, and a high-frequency design of the high-efficiency transmissive PB metasurface.
[53] N. Yu, P. Genevet, M. a Kats, F. Aieta, J.-P. Tetienne, F. Capasso, and Z. Gaburro, Light propagation with phase discontinuities: Generalized laws of reflection and refraction, Science **334**, 333 (2011).
[54] W. T. Chen, K. Yang, C. Wang, Y. Huang, G. Sun, C. Y. Liao, W. Hsu, H. T. Lin, S. Sun, L. Zhou, A. Q. Liu, and D. P. Tsai, High-efficiency broadband metahologram with polarization-controlled dual images, Nano Lett. **14**, 225 (2014).
[55] D. Wen, F. Yue, G. Li, G. Zheng, K. Chan, S. Chen, M. Chen, K. F. Li, P. W. Wong, K. W. Cheah, E. Y. Pun, S. Zhang, and X. Chen, Helicity multiplexed broadband metasurface holograms, Nat. Commun. **6**, 8241 (2015).
[56] M. Kang, J. Chen, X.-L. Wang, and H.-T. Wang, Twisted vector field from an inhomogeneous and anisotropic metamaterial, J. Opt. Soc. Am. B **29**, 572 (2012).